### MSEC2023-104235

### SYSTEMIC CONTROL OF 3D BIOPRINTING PROCESS PARAMETERS TO ACHIEVE DEFINED SCAFFOLD POROSITY

# Connor Quigley Department of Sustainable Product Design and Architecture, Keene State College, Keene, NH.

# Slesha Tuladhar Department of Sustainable Product Design and Architecture, Keene State College, Keene, NH.

# Samrat Adhikari Department of Sustainable Product Design and Architecture, Keene State College, Keene, NH.

# MD Ahasan Habib\* Department of Sustainable Product Design and Architecture, Keene State College, Keene, NH.

#### **ABSTRACT**

Due to its inbuilt ability to release biocompatible materials encapsulating living cells in a predefined location, 3D bioprinting is a promising technique for regenerating patientspecific tissues and organs. Among various 3D bioprinting techniques, extrusion-based 3D bio-printing ensures a higher percentage of cell release, ensuring suitable external and internal scaffold architectures. Scaffold architecture is mainly defined by filament geometry and width. A systematic selection of a set of process parameters, such as nozzle diameter, print speed, print distance, extrusion pressure, and material viscosity, can control the filament geometry and width, eventually confirming the user-defined scaffold porosity. For example, carefully selecting two sets of process parameters can result in a similar filament width. However, the lack of availability of sufficient analytical relations between printing process parameters and filament width creates a barrier to achieving defined scaffold architectures with available resources. In this paper, filament width was determined using an image processing technique and an analytical relationship was developed, including various process parameters to maintain defined filament width variation for different hydrogels within an acceptable range to confirm the overall geometric fidelity of the scaffold. Proposed analytical relations can help achieve defined scaffold architectures with available resources.

#### 1. INTRODUCTION

An emerging technology, bio-printing replicates 3D tissue scaffolds for use in tissue engineering by applying a computer-controlled 3D printing process. Among various most popular bio-printing modalities such as inkjet, extrusion-based, and laser-assisted [1, 2], the third one may deposit a wide variety of substances, including heterogeneous bio-ink [3, 4]. By adjusting the printing parameter, both acellular bio-ink [5, 6] and cell-laden bio-ink [7, 8] have been extruded to form scaffold structures, and good cell survival (>80%) and density [9, 10] are accomplished with this very simple technology.

Scaffolds fabricated with 3D bioprinting process can be directly impacted by the choice of biomaterial, as well as by their rheological and mechanical properties, which permit their desired functionality [11-13]. Additionally, scaffold construction with controlled pore size, porosity, and pore connectivity can aid in simulating the in-vivo microenvironment to promote tissue formation [14, 15]. According to reports, variations in pore size and geometry have an impact on how cells behave within the scaffold structure [16]. However, due to both material and process properties, the extrusion-based bioprinting approach frequently exhibits a large discrepancy between design and manufactured item [17]. As a result, it can be difficult to achieve shape fidelity, biocompatibility, and mechanical integrity inside the scaffold structure. Research is ongoing to find the best biomaterials for fabricating the 3D controlled porous structure utilizing additive manufacturing (bio-AM).

Alginate, gelatin, chitosan, collagen, and fibrin are examples of natural hydrogels that are often utilized in the construction of scaffolds [18]. Polycaprolacton (PCL), polyethylene glycol (PEG), and polylactic acid (PLA) are some synthetic polymers are also used in 3D bioprinting process along with those natural polymers. Due to its biocompatibility and processability, alginate is frequently chosen among them for the construction of scaffolds [24]. However, to achieve the defined shape fidelity and subsequent porosity of 3D printed scaffolds, we researchers depend mostly on appropriate material component and composition selection where we still leave the appropriate process parameters selection unexplored. Most of the time, process parameters are selected based on the selected material [19, 20]. Due to the unavailability of process parameters suitable for selected materials provided by available resources such as air pressure, 3D bioprinter with wide range capabilities, and nozzle size, we may not be able to print defined scaffold architecture. A systematic selection of a set of process parameters (PP), such as nozzle diameter (ND), print speed (PS), print distance (PD), and extrusion pressure (EP) can control the filament geometry and width (FW) and eventually confirming the user-defined scaffold porosity of a material [21] as shown in Figure 1(a). On the other hand, Figure 1(b) shows that the process parameters can be controlled systematically to obtain the filament with similar width using materials having two different viscosities (VIS) [22]. However, the lack of sufficient analytical relations between printing process parameters and filament width creates a barrier to achieving defined scaffold architectures with available resources. In this paper, filament width was determined using an image processing technique and an analytical relationship was developed, including various process parameters to maintain defined filament width variation for different hydrogels within an acceptable range to confirm the overall geometric fidelity of the scaffold. Proposed analytical relations can help achieve defined scaffold architectures with available resources.

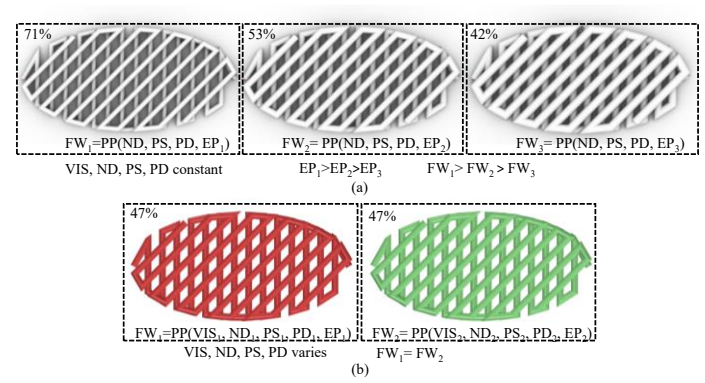


Figure 1: (a) CHANGES OF FILAMENT WIDTH (FW) AND SUBSEQUENT **POROSITIES** APPLYING EXTRUSION PRESSURES (EP) FOR A MATERIAL MAINTAINING NOZZLE DIAMETER (ND), PRINT SPEED (PS), PRINT DISTANCE (PD) CONSTANT. HERE FW INCREASES WITH EP, THEREFORE, **POROSITY** REDUCES FROM 71% TO 42% (b) SIMILAR FW WITH TWO DIFFERENT SETS OF PP FOR TWO DIFFERENT MATERIALS. POROSITY WAS DETERMINED BY (TOTAL VOLUME OF SCAFFOLD- VOLUME OF SOLID) WITH RESPECT TO THE TOTAL VOLUME OF THE SCAFFOLD SHOWN [23].

#### 2. MATERIALS AND METHODS

### 2.1 Processing of materials and process parameters selection

To identify the impact of various process parameters such as EP, PS, ND, and PD on the FW, we used 4% (w/v) Alginate and 4% (w/v) (pH: 6.80) (Sigma-Aldrich, St. Louis, MO, USA) prepared material following protocol described in our previous work [24]. We will denote this material composition as  $A_4C_4$  in this paper. To maintain the filament width similar for two different materials, we used 2% Alginate-6% Carboxymethyl Cellulose (CMC) ( $A_2C_6$ ) and  $A_4C_4$ . We used an extrusion-based 3D bio-printer [BioX (CELLINK, Boston, MA)] to fabricate the filaments and scaffolds. Scaffolds with a dimension of 20mm × 20mm with variational pore sizes i.e., 2 mm × 2mm, 2mm × 8mm, and 8mm × 8mm were fabricated in this paper. We

prepared hydrogels, accordingly, loaded them into a 3.0 ml disposable nozzle, and extruded pneumatically on a stationary build plane. A visual basic-based Computer-Aided Design (CAD) software, Rhino 6.0 (https://www.rhino3d.com), was used to design and define the vectorized toolpath of a scaffold. Slicer (https://www.slicer.org), a G-code generator software was used to generate a Bio-X compatible file including the toolpath coordinates and all process parameters to build the scaffold. We followed a layer-upon-layer fashion to release the materials. For each measurement, three filaments were fabricated. The images of fabricated filaments were captured between 1-2 minutes of printing using the CK Olympus bright field microscope [25] and image were taken at lowest possible time. The width of the filament is determined using ImageJ software.

To identify the impact of various process parameters on filament width, we used 60, 80, 100, 110, 130, 150, and 170 kPa extrusion pressures; PS, ND, and 5, 10, and 15 mm/s print speeds; 210 and 410  $\mu m$  nozzle diameters in this paper. The combination of all process parameters is shown in Figure 2. Print distance, z-height, bed temperature, and print temperature were maintained constant as 150  $\mu m$ , 300  $\mu m$ , 23°C, and 30°C throughout the experiments.

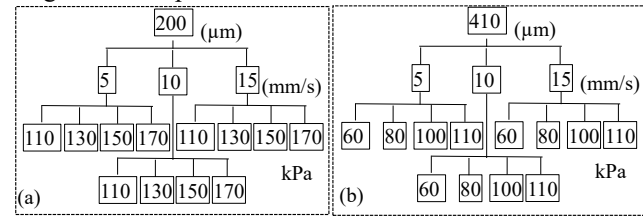


**Figure 2:** THE COMBINATION OF ALL PROCESS PARAMETERS SUCH AS (a) ND:  $200 \mu m$ , PS: 5, 10, 15 mm/s, and EP: 110-170 kPa and (b) ND:  $410 \mu m$ , PS: 5, 10, 15 mm/s, and EP: 60-110 kPa.

To maintain the filament width similar for two different materials, process parameters such as layer height, print speed, extrusion pressure used to fabricate the scaffold were 0.15mm, 5 mm/s, and 110-120 kPa respectively.

#### 2.2 Analysis of the filament width

Filament width was determined using an image analysis method. Images were taken of finished filaments with a microscope within a minute of printing them as shown in Figure 3 (a). The scale of the microscope image was calculated to determine the width of an image. These images were then analyzed using MATLAB (MATHWORKS, Natick, Massachusetts, USA) image batch processing toolbox. Images were loaded into the program, processed and binarized then measured across to find the diameter/width as shown in Figure 3 (b). These measurements were then repeated to find an average diameter for the printed filament. The deviation of filament width from the nozzle diameter it was extruded through was defined as diffusion filament [(actual width-nozzle diameter)/nozzle diameterx 100] of filament in this paper.

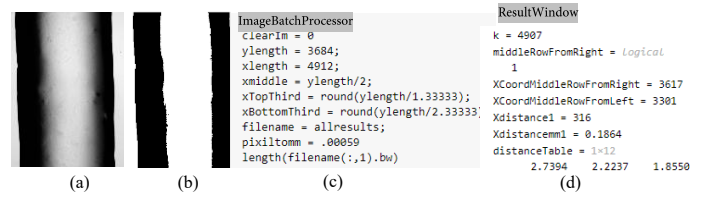


Figure 3: (a) IMAGES WERE TAKEN OF FINISHED FILAMENTS WITH A MICROSCOPE WITHIN A MINUTE OF PRINTING (b) IMAGES WERE LOADED INTO THE PROGRAM, PROCESSED AND BINARIZED, (c) UTILIZING IMAGE BATCH PROCESSING TOOLBOX, AND (d) RESULT WINDOW.

#### 2.3 Statistical analysis

We collected data following a format of "mean  $\pm$  standard deviation" for 250 micron nozzle, 60 and 110 kPa extrusion pressure, and 5, 10, and 15 mm/s print speed; and analyzed them using a significance level of p = 0.05 with a two-way ANOVA. We used a statistical software, Origin Pro 2021b (OriginLab, Northampton, MA) to analyze quantitatively and graphically.

#### 3. RESULTS AND DISCUSSION

#### 3.1 Analysis of filament width

With two nozzles having diameter of 200 µm and 410µm, a total of 24 filaments were fabricated using different extrusion pressures and print speeds as shown in Figure 3 and Figure 4. Filament width for various applied pressures (from 60 kPa to 170 kPa) and print speeds (5, 10, 15 mm/s) extruded through 200 μm and 410 µm is shown in Figure 5. A 3D surface plot was created for filament width with respect to print speed and extrusion pressure for two nozzle diameters as shown in Figure 5. Since, 6 we chose only one material type such as A<sub>4</sub>C<sub>4</sub>, for smaller nozzle (200 μm), we applied higher pressures such as 110kPa, 130kPa, 150kPa, and 170kPa to overcome the internal shear stress created by the nozzle wall to get proper filament shape. For each extrusion pressure, we printed the filament with three different speeds such as 5, 10, and 15 mm/s. It is clear from Figure 4, 6, and 7 that for each extrusion pressure the filament diameter showed a decreasing trend with increasing the print speed. For an example, filament width was reduced 13.37% and 29.15% for print speed of 10mm/s and 15mm/s respectively compared to the filament width fabricated with 5mm/s extruded through 200 µm nozzle applying 110kPa extrusion pressure. Extrusion pressure such as 150kPa and 170kPa were extremely high which created larger filament width compared to the smaller nozzle diameter of 200 µm. Filament width even was getting larger while printed with 5mm/s print speed because of allowing more time for material extrusion. Therefore, filaments fabricated with higher pressure showed a range of filament diffusion rate from 155% (110kPa, 15mm/s) to 736% (150kPa, 5mm/s). This phenomenon indicates that we can achieve larger filament width with smaller nozzle diameter with carefully choosing the extrusion pressure and print speed.

<b>—</b> 0.5 mm	5 mm/s	10 mm/s	15 mm/s
110 kPa			
130 kPa			
150 kPa			
170 kPa			

**Figure 4:** FILAMENTS EXTRUDED THROUGH A 200 μm NOZZLE USING 110, 130, 150, AND 170 kPa EXTRUSION PRESSURE AND 5, 10, AND 15 MM/S PRINT SPEEDS.

On the other hand, we chose lower extrusion pressures such as 60, 80, 100, and 110kPa to extrude the filament through 410  $\mu m$  nozzle. We followed the similar print speeds such as 5, 10, and 15 mm/s for each extrusion pressure and observed for each extrusion pressure the filament diameter showed decreasing trend with increasing the print speed. For an example, filament width was reduced 16.23% and 63.11% for print speed of 10mm/s and 15mm/s respectively compared to the filament width fabricated with 5mm/s extruded through 410  $\mu m$  nozzle applying 80kPa extrusion pressure. Extrusion pressures 100 and 110kPa are extremely higher for a larger nozzle diameter 410  $\mu m$  which created larger filament width as shown in Figure 6 and 7. Therefore, filaments fabricated with higher pressure showed a range of filament diffusion rate from 33.25% (60kPa, 10mm/s) to 346% (110kPa, 5mm/s).

<b>—</b> 0.5 mm	5 mm/s	10 mm/s	15 mm/s
60 kPa			· D.
80 kPa			0
100 kPa			
110 kPa			

**Figure 5:** FILAMENTS EXTRUDED THROUGH A 410 µm NOZZLE USING 60, 80, 100, AND 110 kPa EXTRUSION PRESSURE AND 5, 10, AND 15 MM/S PRINT SPEEDS.

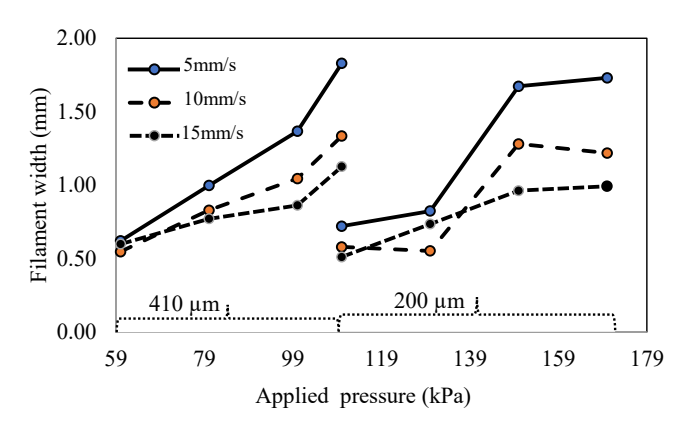


**Figure 6:** FILAMENT WIDTH EXTRUDED THROUGH 200  $\mu m$  AND 410  $\mu m$  NOZZLES AT 5, 10, AND 15 mm/s PRINT SPEED.

Even, in most of the cases, the filament width increases with applied pressure, Figure 6 clearly shows that nozzle with larger diameter such as 410  $\mu m$  performs consistently compared to the nozzle with smaller diameter such as 200  $\mu m$ . Material with higher viscosity intending to extrude through smaller diameter with extensive applied pressure can create interrupted shear stress and result inconsistent outcome.

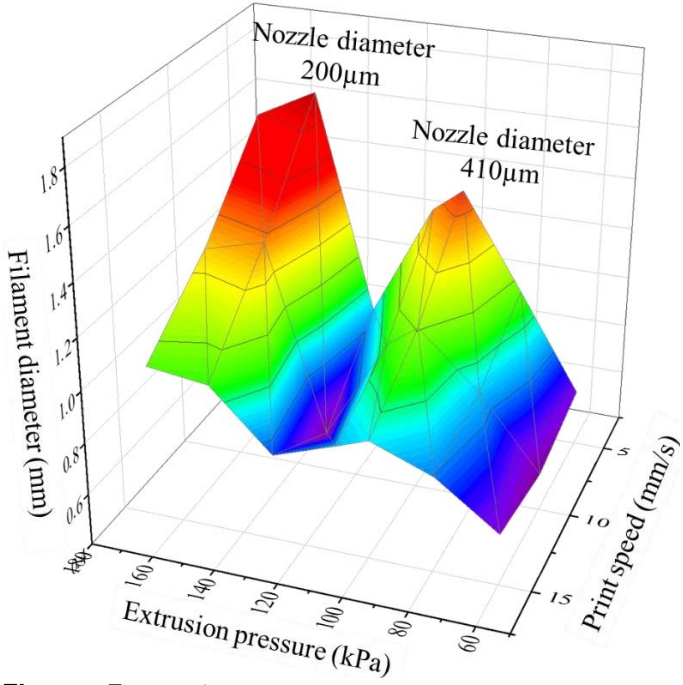


**Figure 7:** A 3D SURFACE PLOT REPRESENTING FILAMENT WIDTH WITH RESPECT TO PRINT SPEED AND EXTRUSION PRESSURE FOR TWO NOZZLE DIAMETERS.

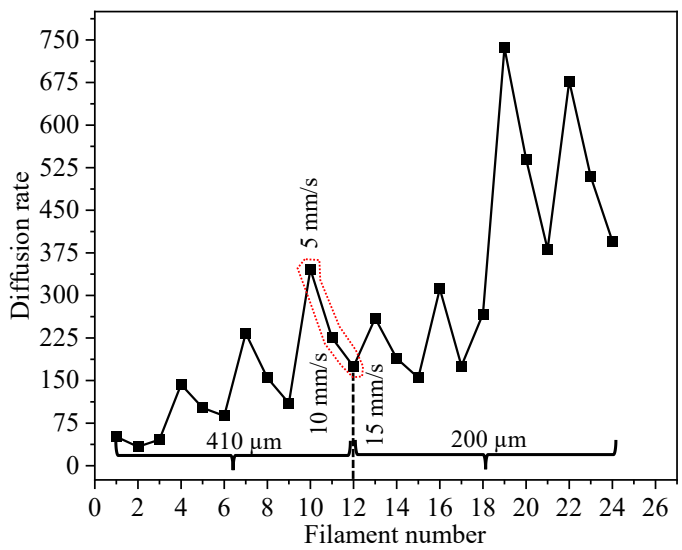


**Figure 8:** DIFFUSION RATE OF EACH FILAMENT: FILAMENT NUMBER 1-12 WAS FABRICATED THROUGH 410  $\mu m$  NOZZLE AND FILAMENT NUMBER 13-24 WAS FABRICATED THROUGH 200  $\mu m$  NOZZLE. THREE ENCIRLED POINTS REPRESENT THE DIFFUSION RATE OF FILAMENT FABRICATED AT 5, 10, AND 15 mm/s AND IT IS SAME FOR ALL GROUPS OF 1-3, 4-6 AND SO ON.

We observed a similar filament width (0.55 mm and 0.57) showing a 3.6% difference fabricated with two different sets of process parameters such as (410 $\mu$ m, 60kPa, 10mm/s) and (200 $\mu$ m, 110kPa, 5mm/s). This interesting phenomenon indicates that we can achieve similar filament width by carefully selecting the available process parameters and resources. With an exhaustive search we found a set of combinations of process parameters for 200  $\mu$ m and 410  $\mu$ m nozzle diameters that can create filament width showing a difference from 0.64% to 7.6% as shown in Table 1.

**Table 1:** A SET OF COMBINATIONS OF PROCESS PARAMETERS THAT CREATED SIMILAR FILAMENT WIDTH WITH SHOWING DIFFERENCE FROM 0.64% TO 7.6%.

Process p	% of difference	
410µm, 60kPa, 10mm/s	$200\mu m,110kPa,10mm/s$	5.5
$410\mu m,60kPa,15mm/s$	$200\mu m,110kPa,10mm/s$	3.46
$410\mu m,80kPa,10mm/s$	$200\mu m,130kPa,5mm/s$	0.64
$410\mu m,100kPa,5mm/s$	$200\mu m,170kPa,10mm/s$	6.72
$410\mu m,100kPa,10mm/s$	$200\mu m,170kPa,15mm/s$	5.35
410µm, 110kPa, 15mm/s	200μm, 170kPa, 10mm/s	7.6

To demonstrate significance of the difference statistically, we conducted a two-sample t-test considering known variance and resulting p-value was 0.023(<0.05). Therefore, with 95% confidence interval, we failed to reject the null hypothesis meaning they do not have significant differences. The difference we observed was due to random reason.

#### 3.2 Multiple regression

To determine an analytical relation between filament diameter and related process parameters such as extrusion pressure, nozzle diameter, print speed, we used multiple linear regression method. First of all, we conducted a multiple linear regression analysis for the filaments fabricated with  $410\mu m$  and found the following relation:

$$FW = -0.0152 + 0.0156EP - 0.036PS \tag{1}$$

We observed an adjusted R- square value 83.62% meaning the relation we obtained can explain the 83.62% variance of the filament width can be explained by variance of independent variables, extrusion pressure and print speed.

Then we conducted a multiple linear regression analysis for the filaments fabricated with 200  $\mu m$  and found the following relation:

$$FW = -0.43 + 0.0128 EP - 0.039PS \tag{2}$$

In this regression analysis, we observed an adjusted R- square value 72% meaning the relation we obtained can explain the 72% variance of the filament width can be explained by variance of independent variables, extrusion pressure and print speed. Therefore, it can be concluded that filament width can be predicted better for larger nozzle diameter than smaller diameter. The filament diffusion rate shown in Figure 8 also supports this. The prediction of filament width fabricated with 200  $\mu m$  and 410  $\mu m$  nozzles with respect to extrusion pressure and print speed is shown in Figure 9. However, the probability for interception was 0.95 and 0.31 for nozzle 410  $\mu m$  and 200  $\mu m$  respectively which is greater than the 0.15 meaning that interception is not significant to predict the filament width with respect to extrusion pressure and print speed.

We then added nozzle diameter as third variable along with extrusion pressure and print speed and conducted multiple regression analysis to predict the filament with. We also considered the following interactions: (EP, PS), (EP, ND), (PS, ND), and (EP, PS, ND) during the analysis and we got the following relation:

$$FW = -2 + 0.01365EP + 0.075PS + 1.986ND - 0.000362(EPxPS) + 0.0378(EPxND) + 0.0132(PSxND) - 0.0024(EPxPSxND)$$
 (3)

In this case, we achieved an adjusted R-seq value 82.8%. However, the p-value for each interaction variable was greater than 0.15 indicates that they do not impact the filament width significantly. Therefore, we removed the interaction effect and conduct the regression analysis again and got the following relationship:

$$FW = -1.3445 + 0.014EP - 0.0386PS + 3.63ND$$
 (4)

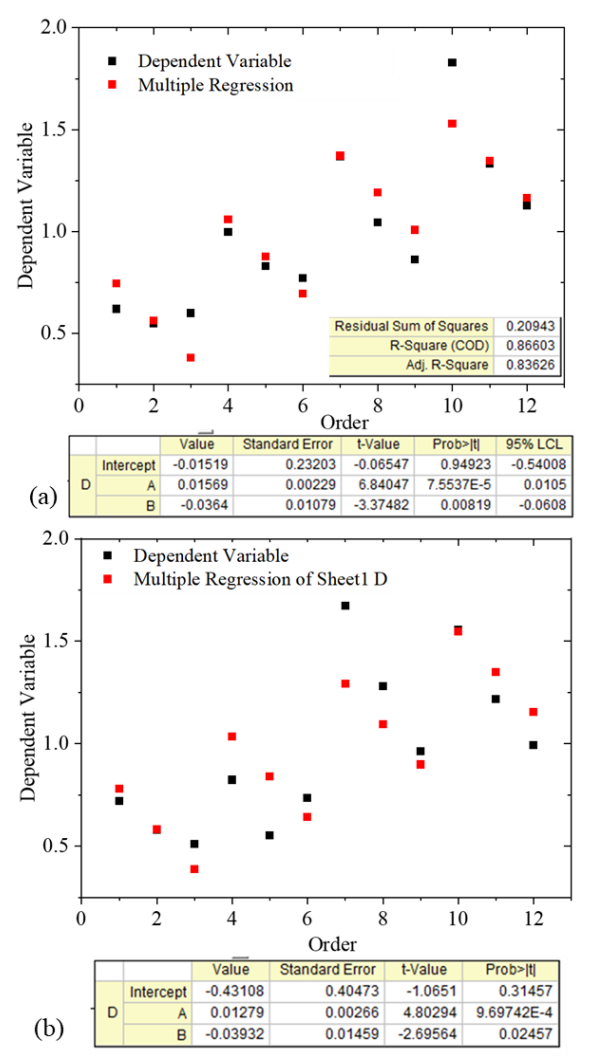


**Figure 9:** PREDICTION OF FILAMENT WIDTH WITH RESPECT TO EXTRUSION PRESSURE AND PRINT SPEED FOR NOZZLE (a) 410 µm (b) 210 µm.

In this case, we achieved an adjusted R-seq value 78.2% as shown in Figure 10 which is greater than the adjusted R-square value we got for 200  $\mu m$  nozzle diameter. The probability value for interception, extrusion pressure, print speed, and nozzle diameter is less than 0.15 meaning all of them are significant to predict the filament width. To validate the model shown in Equation 4, we fabricated two filaments with two different sets of process parameters such as (610 $\mu m$ , 82kPa, 10mm/s) and (250 $\mu m$ , 80kPa, 5mm/s) considering other parameters such as print distance, z-height, and bed temperature constant. Experimental data showed 14% and 16% difference respectively with respect to the predicted data.

In all multiple regression models from Equation (1-4), the constant represents the predicted value for the filament width if all the independent variables such as EP, PS, and ND were simultaneously equal to zero. This situation does not represent any physical or economical meaning. Since, users may not be specifically interested in the result if EP, PS, and ND were simultaneously zero, we normally leave the constant in the model regardless of its statistical significance. This constant also ensures the unbiasedness of sample errors allowing

the regression model to seek its own level and provide the best fit to data.

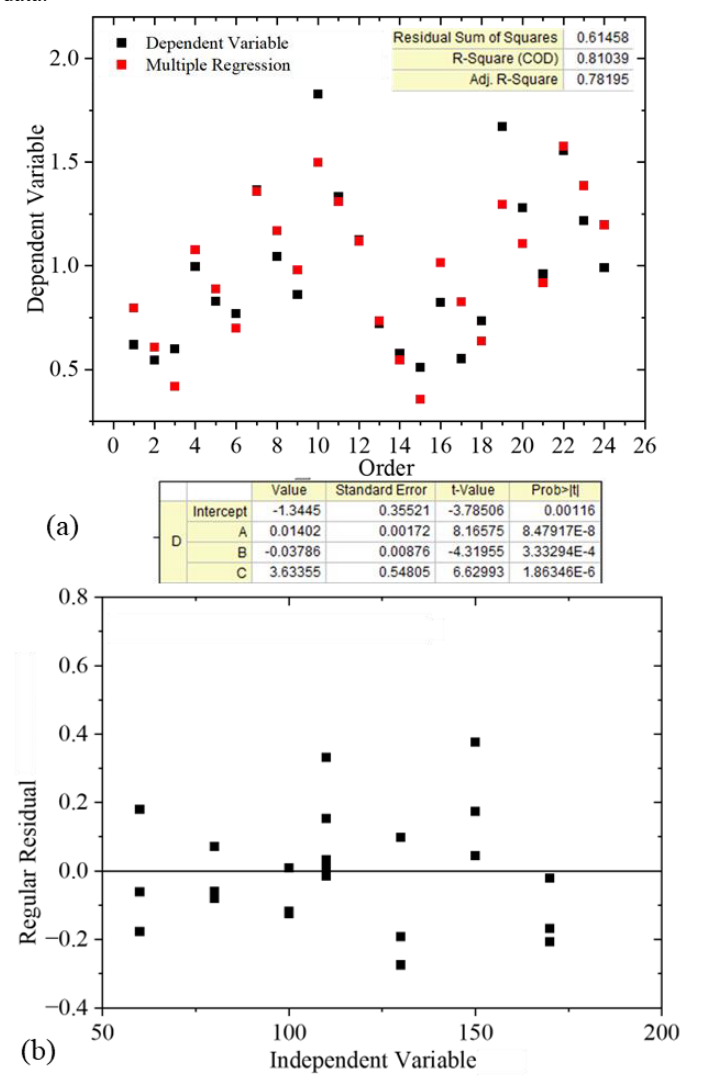


**Figure 10:** (a)PREDICTION OF FILAMENT WIDTH WITH RESPECT TO EXTRUSION PRESSURE, PRINT SPEED, AND NOZZLE DIAMETER. WE OBSERVED AN ADJSUTED R-SQUARE VALUE OF 78.2%. (b) DISTRIBUTION OF REGULAR RESIDUALS WITH RESPECT TO INDEPENDENT VARIABLE.

This research demands good amount of time and resources. Therefore, it is still on-going. To demonstrate the repeatability, we tested comparatively a small sample numbers where the filaments were fabricated through 250  $\mu m$  diameter applying 60 and 110 kPa extrusion pressure at 5, 10, and 15 mm/s as shown in Figure 11. The statistical analysis (n=3) represents a non-significant difference of filament width for each process parameters combinations. In future, we will fabricate three samples for each combination as shown in Figure 2.

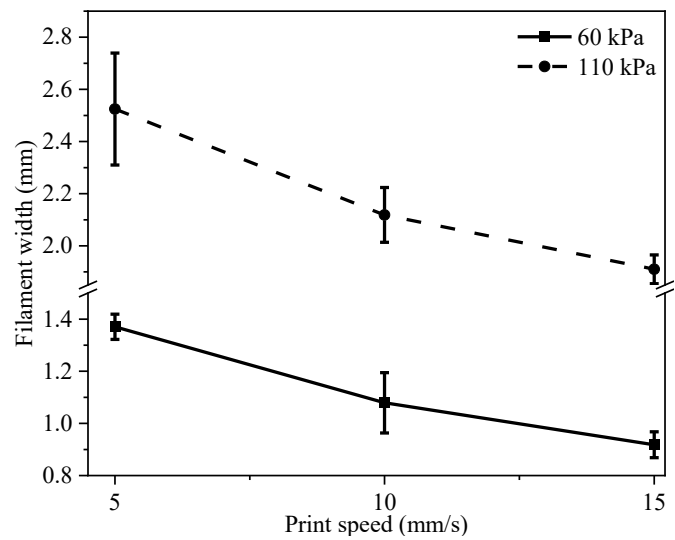


**Figure 11:** FILAMENT DIAMETER FABRICATED THROUGH 250 μm DIAMETER APPLYING 60 AND 110 KPa EXTRUSION PRESSURE AT 5, 10, AND 15 mm/s.

#### 3.3 Analysis of filament width for various viscosities

In this section, we have added material viscosity as another variable to analyze the filament width with various process parameters mentioned in section 2.1. A<sub>2</sub>C<sub>6</sub> along with A<sub>4</sub>C<sub>4</sub> was considered demonstrate that the process parameters can be controlled systematically to obtain the filament with similar width from two different materials. Two scaffolds were fabricated following similar process parameters except 10kPa higher extrusion pressure for A<sub>2</sub>C<sub>6</sub> as shown in Figure 12. Since the viscosity of A<sub>2</sub>C<sub>6</sub> is higher than A<sub>4</sub>C<sub>4</sub> [22], the former material composition took higher extrusion pressure (120kPa) to maintain the filament width constant. Microscopic view presented only 5% variation of the filament width for scaffolds fabricated with A<sub>2</sub>C<sub>6</sub> and A<sub>4</sub>C<sub>4</sub>.

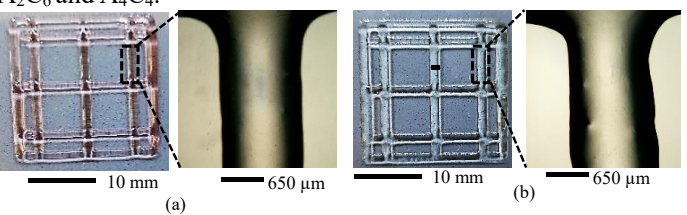


Figure 12: SCAFFOLDS FABRICATED WITH (A)  $A_2C_6$  and (B)  $A_4C_4$  hydrogels with two different sets of Printing Parameters represents similar filament width.

#### 4. CONCLUSION

From this paper, it is clear from the results that a systematic selection of process parameters can help fabricate scaffold with a defined filament width which eventually confirms the defined shape fidelity of the scaffold. The adjusted R-square value for a regression model predicting the filament width with respect to extrusion pressure, print speed, and nozzle diameter was identified 78.2%. Including more experimental data can improve this co-relation value. In future, we plan to include the experimental data for

nozzles of 250  $\mu m$  and 610  $\mu m$  maintaining similar extrusion pressure and print speeds. Moreover, we also plan to explore a machine learning algorithm such Support Vector Machine (SVM) with increasing amount of experimental data to identify a strong predictive model so that we can fabricate defined filament width with available resources. Successfully achieving this long-term goal can take the extrusion-based 3D bioprinting technique one step ahead to fabricate patient-specific tissue scaffold.

#### **ACKNOWLEDGEMENTS**

Research was supported by New Hampshire-EPSCoR through BioMade Award #1757371 from National Science Foundation and New Hampshire-INBRE through an Institutional Development Award (IDeA), P20GM103506, from the National Institute of General Medical Sciences of the NIH.

#### **REFERENCES**

- [1] S. V. Murphy and A. Atala, "3D bioprinting of tissues and organs," *Nature biotechnology*, vol. 32, no. 8, pp. 773-785, 2014.
- [2] Y. He, F. Yang, H. Zhao, Q. Gao, B. Xia, and J. Fu, "Research on the printability of hydrogels in 3D bioprinting," *Scientific reports*, vol. 6, p. 29977, 2016.
- [3] S. Ji and M. Guvendiren, "Recent advances in bioink design for 3D bioprinting of tissues and organs," *Frontiers in bioengineering and biotechnology*, vol. 5, p. 23, 2017.
- [4] K. Hölzl, S. Lin, L. Tytgat, S. Van Vlierberghe, L. Gu, and A. Ovsianikov, "Bioink properties before, during and after 3D bioprinting," *Biofabrication*, vol. 8, no. 3, p. 032002, 2016.
- [5] V. C.-F. Li, C. K. Dunn, Z. Zhang, Y. Deng, and H. J. Qi, "Direct Ink Write (DIW) 3D Printed Cellulose Nanocrystal Aerogel Structures," *Scientific Reports*, vol. 7, no. 1, p. 8018, 2017.
- [6] C. R. Almeida, T. Serra, M. I. Oliveira, J. A. Planell, M. A. Barbosa, and M. Navarro, "Impact of 3-D printed PLA-and chitosan-based scaffolds on human monocyte/macrophage responses: unraveling the effect of 3-D structures on inflammation," *Acta biomaterialia*, vol. 10, no. 2, pp. 613-622, 2014.
- [7] J. H. Chung *et al.*, "Bio-ink properties and printability for extrusion printing living cells," *Biomaterials Science*, vol. 1, no. 7, pp. 763-773, 2013.
- [8] A. G. Tabriz, M. A. Hermida, N. R. Leslie, and W. Shu, "Three-dimensional bioprinting of complex cell laden alginate hydrogel structures," *Biofabrication*, vol. 7, no. 4, p. 045012, 2015.
- [9] J. Jia *et al.*, "Engineering alginate as bioink for bioprinting," *Acta biomaterialia*, vol. 10, no. 10, pp. 4323-4331, 2014.
- [10] L. Ouyang, R. Yao, Y. Zhao, and W. Sun, "Effect of bioink properties on printability and cell viability for

- 3D bioplotting of embryonic stem cells," *Biofabrication*, vol. 8, no. 3, p. 035020, 2016.
- [11] I. T. Ozbolat, A. Khoda, M. Marchany, J. A. Gardella, and B. Koc, "Hybrid tissue scaffolds for controlled release applications: A study on design and fabrication of hybrid and heterogeneous tissue scaffolds for controlled release applications is presented in this paper," *Virtual and Physical Prototyping*, vol. 7, no. 1, pp. 37-47, 2012.
- [12] K.-S. Han *et al.*, "Effect of pore sizes of silk scaffolds for cartilage tissue engineering," *Macromolecular Research*, vol. 23, no. 12, pp. 1091-1097, 2015.
- [13] A. Gottipati and S. Elder, "Effect of Chitosan Calcium phosphate Bead size on Scaffold Properties as they relate to Formation of Biphasic Constructs for Osteochondral Regeneration," *Journal of Polymer Materials*, vol. 34, no. 1, p. 287, 2017.
- [14] C. M. Murphy, M. G. Haugh, and F. J. O'Brien, "The effect of mean pore size on cell attachment, proliferation and migration in collagen—glycosaminoglycan scaffolds for bone tissue engineering," *Biomaterials*, vol. 31, no. 3, pp. 461-466, 2010.
- [15] R. A. Perez and G. Mestres, "Role of pore size and morphology in musculo-skeletal tissue regeneration," *Materials Science and Engineering: C*, vol. 61, pp. 922-939, 2016.
- [16] N. Vargas-Alfredo, A. Dorronsoro, A. L. Cortajarena, and J. Rodríguez-Hernández, "Antimicrobial 3D Porous Scaffolds Prepared by Additive Manufacturing and Breath Figures," *ACS Applied Materials & Interfaces*, vol. 9, no. 42, pp. 37454-37462, 2017.
- [17] A. Khoda, I. T. Ozbolat, and B. Koc, "Engineered tissue scaffolds with variational porous architecture," *Journal of Biomechanical Engineering*, vol. 133, no. 1, p. 011001, 2011.
- [18] C. C. Chang, E. D. Boland, S. K. Williams, and J. B. Hoying, "Direct-write bioprinting three-dimensional biohybrid systems for future regenerative therapies," Journal of Biomedical Materials Research Part B: Applied Biomaterials, vol. 98, no. 1, pp. 160-170, 2011.
- [19] Z. M. Jessop *et al.*, "Printability of pulp derived crystal, fibril and blend nanocellulose-alginate bioinks for extrusion 3D bioprinting," *Biofabrication*, vol. 11, no. 4, p. 045006, 2019/07/08 2019, doi: 10.1088/1758-5090/ab0631.
- [20] A. Ribeiro *et al.*, "Assessing bioink shape fidelity to aid material development in 3D bioprinting," *Biofabrication*, 2017.
- [21] H. Ding and R. Chang, "Printability study of bioprinted tubular structures using liquid hydrogel precursors in a support bath," *Applied Sciences*, vol. 8, no. 3, p. 403, 2018.
- [22] C. Quigley, S. Tuladhar, and A. Habib, "A Roadmap to Fabricate Geometrically Accurate Three-Dimensional Scaffolds CO-Printed by Natural and Synthetic

- Polymers," *Journal of Micro-and Nano-Manufacturing*, vol. 10, no. 2, p. 021001, 2022.
  Q. L. Loh and C. Choong, "Three-dimensional
- [23] Q. L. Loh and C. Choong, "Three-dimensional scaffolds for tissue engineering applications: role of porosity and pore size," *Tissue Engineering Part B: Reviews*, vol. 19, no. 6, pp. 485-502, 2013.
- [24] A. Habib, V. Sathish, S. Mallik, and B. Khoda, "3D printability of alginate-carboxymethyl cellulose hydrogel," *Materials*, vol. 11, no. 3, p. 454, 2018.
- [25] R. S. Kumar V, Cutkosky M, Dutta D, "Representation and processing heterogeneous objects for solid freeform fabrication," ed. Sixth IFIP WG 5.2 International Workshop on Geometric Modelling: Fundamentals and Applications, Tokyo, Japan, The University of Tokyo, 1998.